ORIGINAL ARTICLE

Analysis of the hot radial forging process according to the finite element method

Saeed Darki[1] · Evgeniy Yurevich Raskatov[1]

Abstract

The radial forging process (RFP) is an advanced technology that many scientists have recently been trying to optimize and improve in order to enhance the quality of products and save energy in manufacturing. However, controlling the process when employed on large products is very difficult due to the appearance of cracks. During RFP, a tube is repeatedly and continuously exposed to stroking and feeding. Thus, when the die comes into contact with the product, the rotational feed stops. Afterwards, when the hummers break contact with the tube, the axial and rotational feeds are applied simultaneously in order to obtain a good surface finish at a specific rotation angle feed. Implementing RFP is a costly and lengthy process largely done through trial and error. It depends on variables such as material temperature, rotation speed, rate of feed, parameters of die geometry, die pressure, and amplitude. Thus, a symmetric 3D model simulation has been conducted with commercial FEM software. The results include the cantors of residual stress (RS), strain velocity, and temperature. Equally, the contact forces have been measured as experimental results, and there is a good correspondence between the two types of results.

Keywords Three-dimensional finite element method · Tube diameter reduction · Radial forging · Residual stress

1 Introduction

Hot radial forging is a particular form of the open forging process. Based on this process, a tube or hollow shaft is deformed across four dies and one mandrel, which increases the stiffness of the product and changes its radius. Open forging is mainly used to reduce the dimeter of ingots made from special alloys. Consequently, radial die forging is a costly and complex process. Recently, many scientists have studied RFP to obtain benefits such as decreased process costs, material


Highlights
- A RFP simulation has been carried out with 3D FEM software.
- In terms of material analysis, the viscoplastic model has been assumed.
- The ranges of RS, total strain, and total force have been calculated.
- The results can be implemented in the forging operations to refine the final characteristics of the workpiece.

✉ Saeed Darki
saeed.darki@yahoo.com

Evgeniy Yurevich Raskatov
e.j.raskatov@urfu.ru

[1] New Material and Technology Institute, Ural Federal University, Ekaterinburg, Russia

savings, increased product quality and quantity, and improved process parameters.

Before the current study, other scientists studied RFP in terms of rigid plastic formulation in order to investigate RS. Ameli and Movahhedy [1] developed a cold type of RFP through axisymmetric and 3D-FEM modelling in order to provide the stress rate and die pressure on a tube with grooves. They state that an axisymmetric simulation matches the experimental results; however, due to the type of forging, this model is unable to describe all effective parameters during simulation of the process, especially for temperature and material flow velocity analysis. Angelov and Nedev [2] found a penalty relation based on Coulomb's friction law, which was used to relate the roll pressure and the normal velocities to the contact interface. Thus, they used a velocity-dependent equation to modify friction equations to describe contact forces. Charni et al. [3] studied the causes of RS during the swaging process. They exhibited that the distribution of RS within two directions of radial and axial mainly depends on friction type. Thus, the results showed the range of RS in dry conditions has a higher average than that in wet ones. They claimed the dry process has more longitudinal variation in the axial direction while the roughness of the surface will be increased through the dry forging in comparison with a wet process. Chen et al.

Fig. 1 A schematic of the radial forging process
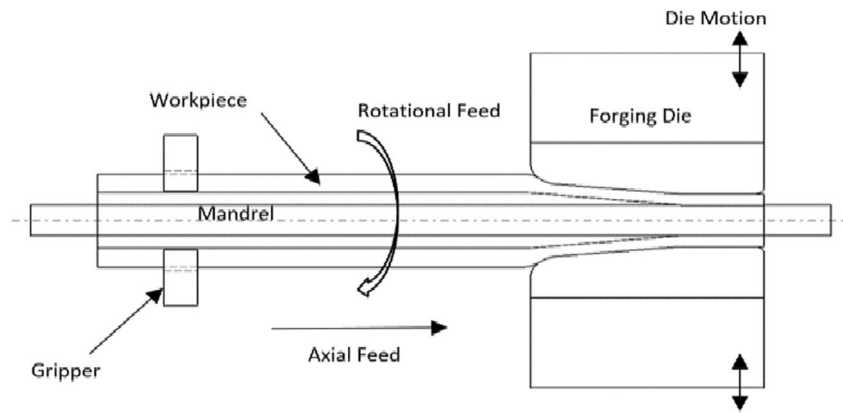
[4] developed a hot type of RFP by FEM. Based on this, they expressed the plastic strain distribution for different percentages of radial reduction for RFP. In addition, they claimed that the use of Mandrel and V-shape die type could have a better performance in reducing the diameter and thickness of the tube and increasing the mechanical properties quality of the tube compared with other Forging conditions. Choi et al. [6] investigated an open forge operation in the manufacture of a circular shape. This investigation was optimized to balance between feed rate forging productivity and the quality of the product. Thus, to create a surface with the maximum quality, the feed rate should be 0.6 diameters of the final product. Fajoui et al. [7] analyzed the mechanical behavior of hot steels based on RS. According to the results, RS is created during the heat treatment and machining processes. It is necessary to mention that the RS generated during machining has a greater effect material. Fan et al. [8] presented rotational and axial feeding based on 2D and 3D simulations. This investigation illustrated the influence of spring push back and spindle speed on the forging load. Given that peripheral deformation is affected by rotational feed, the implementation of a 3D simulation model is necessary. Ghaei et al. [10] developed the slab method of analysis for modelling. Consequently, the deformation pattern and stress distribution were obtained in two different conditions—with the mandrel and without it. They stated its use (or lack thereof) can only affect surface quality. Huang et al. [12] analyzed a comprehensive dynamic process for developing hot RFP, with a focus on complex process kinematics, thermo-viscoplastic material behavior, and RS. They argue that a crack in a stress field can rapidly propagate in products. Jang and Liou [13]

calculated RS for a hollow shaft with a mandrel via a nonlinear 3D simulation. According to this model, Coulomb's law of friction has been assumed between the components of the process in order to describe the contact force. Thus, the values of RS on different layers of the tube were calculated. They used an elastoplastic model to describe material flow. However, this type of simulation is incapable of expressing an accurate estimate of material flow. Karunathilaka et al. [14] studied the efficacy of forge operations on the longevity of tools in terms of fatigue. Using the results, there is a direct relationship between dimension changes, surface hardness, and interface pressure. As contact pressure increases, the longevity of the tool will decrease; thus, die fatigue is enhanced. Khayatzadeh et al. [15] simulated the process via a 3D FEM model of two types of shaft based on multi-pass forging. As claimed by this investigation, the results demonstrate the highest range of strain occurred on the outer surface while the pattern of strain distribution for both types of the sample was approximately the same. Koppensteiner and Auer [16] presented a new RFP system with an elliptic drive shaft and double stroke. According to this innovation, they increased the quality of the surface and the dimension accuracy of products. This new design is based on an elliptical shaft shape that rotates between two rams, one of which is constant and the other with reciprocal movement. Markov et al. [17] developed a new approach to radial open die forging on the stress state. They presented new die schemes that allow for the elimination of the upsetting operation during hot radial forging. Also, the variations
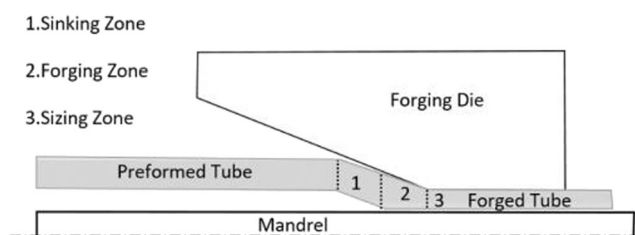
Table 1 Parameters of material in the simulation of the radial forging process

Density (kg/m3)	7870
Young's modulus (GPa)	212
Poisson's ratio	0.3
Specific heat (J/kg/C)	750
Conductivity (W/m/C)	15
Inelastic heat fraction	0.9
Thermal expansion coefficient (1/C)	11×10^{-5}

Fig. 2 Three typical zones of the radial forging process
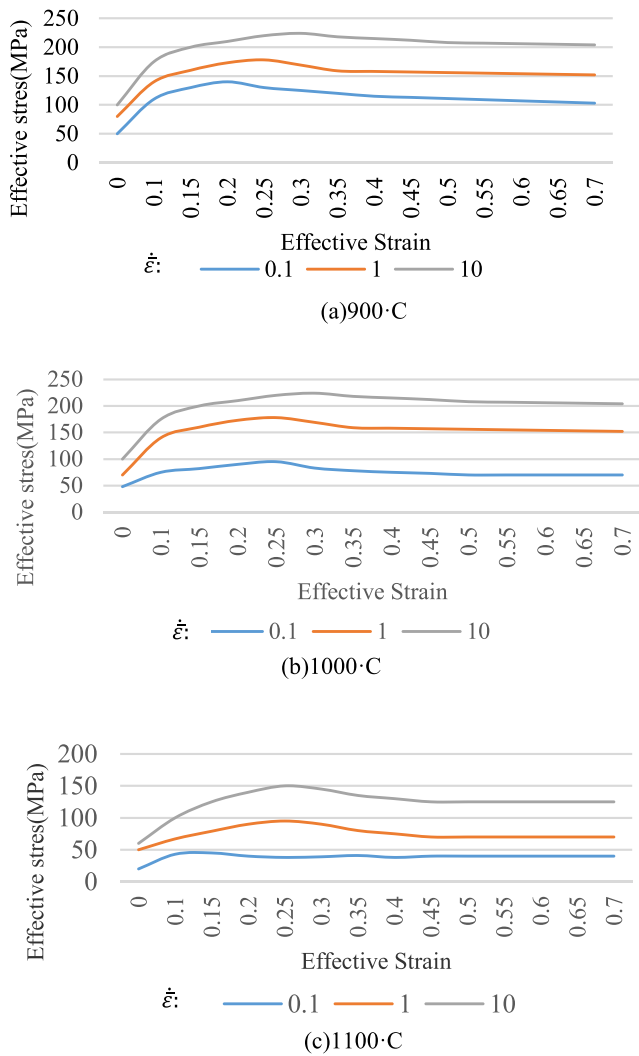
(a)900·C

(b)1000·C

(c)1100·C

Fig. 3 **a**, **b**, **c** Stress-strain curve of DIN-16CrMo4

in the die convex angle can change the number of strokes, contact force, and range of stress. Equally, they noted that the amplitude of the die should be between 160 and 170 degrees. Quagliato et al. [18] investigated RFP for aluminum materials when producing bearings. The distribution and cantor of different types of stress were shown. They also claimed that the total weight of the bearing can be lowered by 35.8% through the new approach.

Table 2 Geometry parameters of the mandrel, workpiece, and die

Outer diameter – before forging (mm)	30
Inner diameter – before forging (mm)	10
Outer diameter – after forging (mm)	24
Inner diameter – after forging (mm)	4
Outer diameter for mandrel (mm)	4
Length of die (mm)	70
Length of die land (mm)	25
Die angle	5·

Table 3 Motion of simulation parameters

Rate of stroking (stroke per min)	400
Rotating feeds	36
Axial feed (mm)	20
Number of strokes	12
Number of pass	2
Rotation per pass	5·

Sanjari et al. [19] predicted the neutral plane and the influence of process factors by using an upper boundary solution. They claimed that the geometrical dimensions of the die cause variations in total force. Moreover, they state that as the friction coefficient increases, the natural plane shifts to the forging zone. This phenomenon causes an increase in the total force for forging. Sanjari et al. [20] determined the strain field in RFP by using a micro hardness test. They utilized different die shapes to investigate their influence on strain distribution. As the push back force increases, the inhomogeneity factor will be increased. Also, if the die angle is increased, then the extra strain will be reduced. Wu et al. [21] found the material flow of cold forging through an analysis of the upper boundary of the longitudinal direction. They used an axisymmetric model to obtain the vectors of the flow material, showing that variation in the product cross-section will change the forward material flow direction. These results are more visible when using a low axial feed. In order to enhance the efficiency of this model, it is necessary to take into account the interaction of changes in die angle on RS for different segments of the process; however, this study neglected to do this.

The aim of the current investigation is to present one numerical model of RFP to analyze and predict all the features of the workpiece after the end of the process. On the other hand, to achieve a reliable and practical method for RFP, all the effective parameters within the process have been applied. Hence, according to previous studies, FEM is the most accurate method to apply all operating conditions and observe the actual condition of the workpiece after the process. The process is completely automated and has a high capability to produce highly accurate parts with high levels of tolerance and a good smooth surface. It also allows for the improvement of the final product's mechanical properties and a high production rate at a low cost. These features have wide application potential in various industrial fields. In the current simulation, the

Table 4 Contact parameters

Friction factor between workpiece and die	0.4 shear
Friction factor between workpiece and mandrel	0.4 shear
Friction factor between workpiece and manipulators	10.0 shear

Table 5   Mesh type and element number for different parts

Part	Mesh type	Elements	Nodes	Size ratio
Workpiece	Tetrahedral	28,532	6450	3
Die	Tetrahedral	29,466	6632	3
Mandrel	Tetrahedral	15,119	4113	3

commercial 3D-Deform software (based on FEM) has been used to simulate RFP. Measurement through accessible empirical outcomes and numerical solution values has also been conducted. The influence of friction parameters on contact force, stresses, and equivalent strain rates is illustrated and discussed.
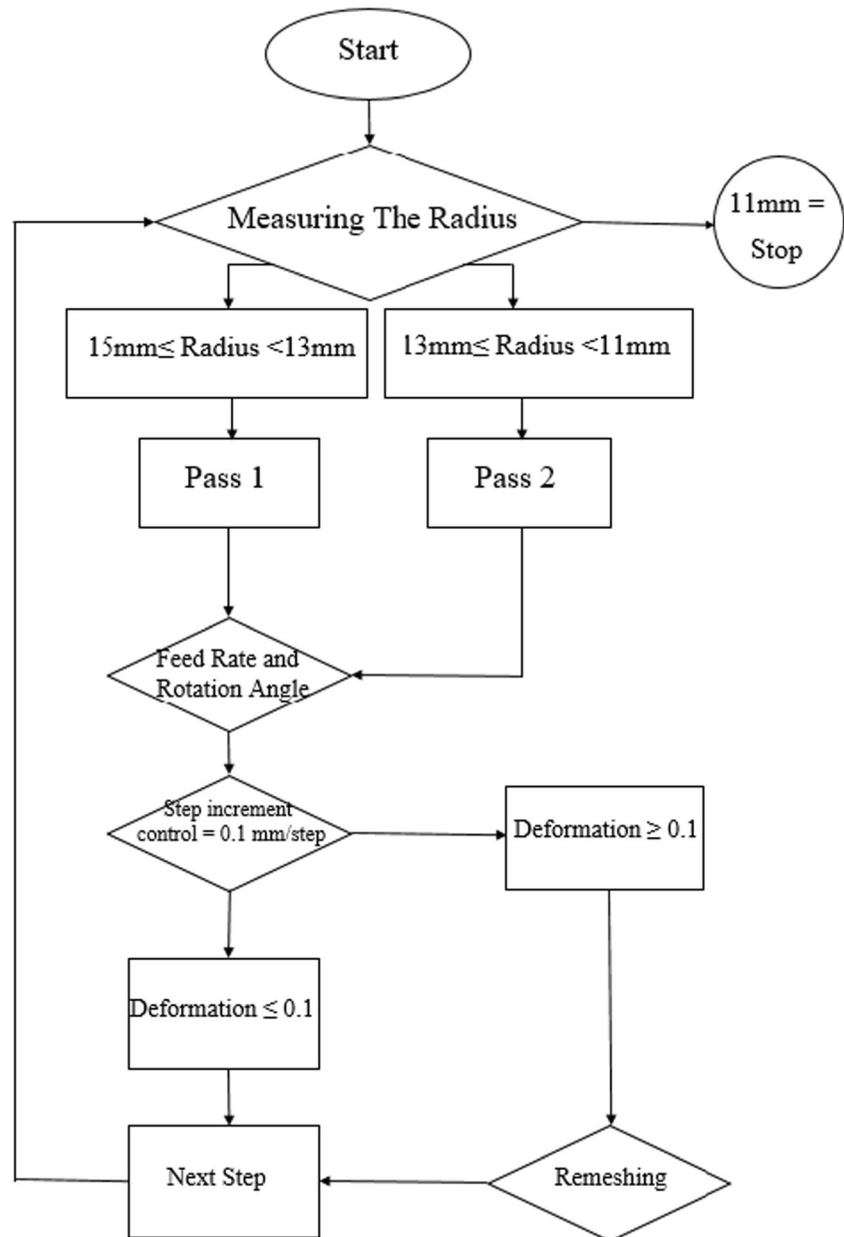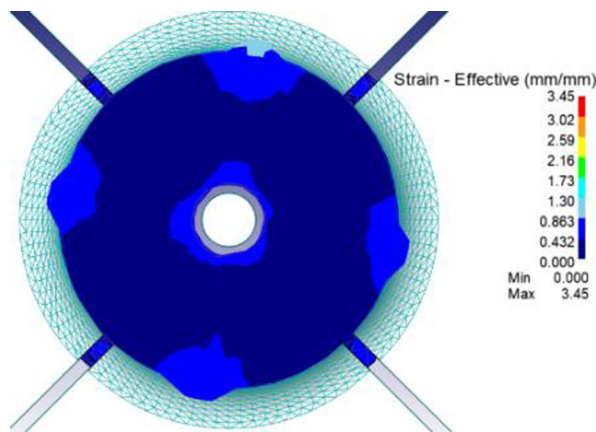
2 Radial forging process and residual stress distribution

A simplified view of RFP components is shown in Fig. 1. The process includes four dies placed around a tube that acts with a specified frequency on the product. It continuously moves at two axial and radial feeding rates. Due to the intrinsic properties of this process, the tube has a large quantity of RS, which causes changes in the tube's dimensions and reduces its tolerance. The residual stress due to RFP has been studied through experiments and numerical simulation. It should be noted that experimental procedures are expensive and time-consuming.
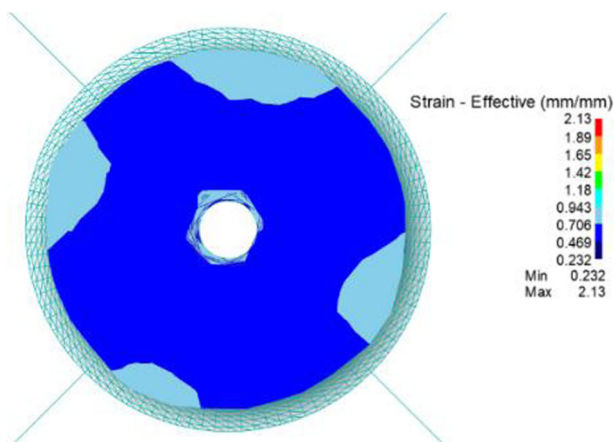
As shown in Fig. 2, Chen et al. [5] gave a schematic model to explain the deformation of products within the forging

Fig. 4 FEM simulation model derivation process

process. In this figure, RFP has been defined in three deformation zones of the product: (i) sinking zone, (ii) forging zone, and (iii) sizing zone. The sinking zone comprises a small amount of deformation. Deformation increases in the forging zone up to maximum value. Compared with the mid-point of the surface, significant deformations occur at the end of the tube on the outer and inner surfaces.

In this investigation, the subjects were investigated via a 3D simulation according to the following conditions: (a) the deformation has been calculated at several passes and each stroke action; (b) the frictional effects have been investigated at the interface of the die and the product. There are the frictional stresses which depend on factors related to the product

according to die geometry; and (c) RS effects for all the steps and final part of the operation have been calculated.

In order to measure and calculate RS and to avoid increases in fatigue, studying RFP is essential. Equally, analysis of and improvements to RFP are used to control process parameters, such as high efficiency in energy consumption. In most previous investigations, an elastoplastic model has been used to examine RFP. Other scientists have investigated RFP but they neglected many details of radial forging. The current research concentrates on the most principal details that play the main role in increasing the accuracy of RFP modelling. Thus, the viscoplastic behavior of the material has been assumed in this simulation. Also, it is necessary to use the modified equations to describe to be a time-dependent process. Transient and thermomechanical coupled problems were considered with the purpose of optimizing the feed rate angle of rotation, temperature, time, number of stroke and passes, and other important factors of operations.

The material used in the simulation is DIN-16CrMo4 steel. The material parameters are expressed in Table 1 at an initial forging temperature of 900 °C. For the current study, flow stress has been obtained by $\overline{\sigma} = \overline{\sigma}(\overline{\varepsilon}, \overline{\varepsilon}\cdot, T)$ (the flow stress ($\overline{\sigma}$) of DIN-16CrMo4 steel). Strain function ($\overline{\varepsilon}$), strain rate ($\dot{\overline{\varepsilon}}$) and temperature ($T$) are also expressed in Fig. 3.

Pass 1 after 2 strokes: a distance of 40 mm.

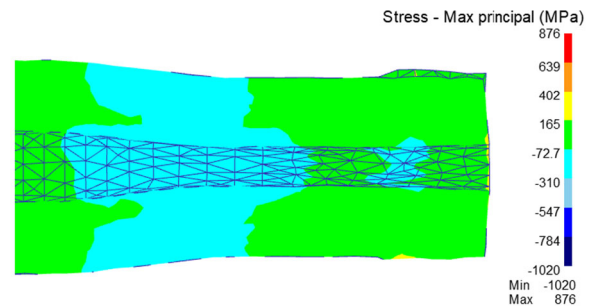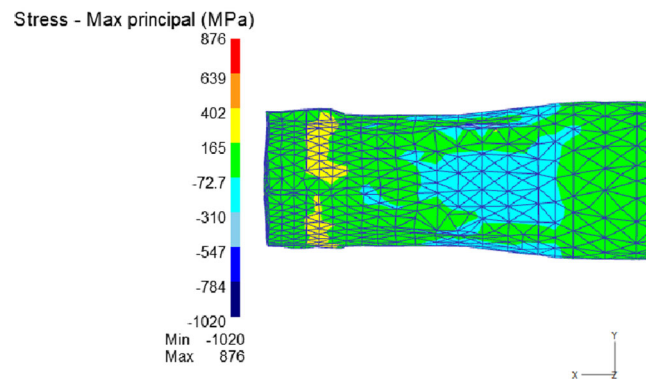
Pass 2 after 2 strokes: a distance of 40 mm.

Fig. 5 Effective strain of cross-section of different stokes. Pass 1 after 2 strokes: a distance of 40 mm. Pass 2 after 2 strokes: a distance of 40 mm

(a)   Inner maximum principal stress.

(b)   Outer maximum principal stress.

Fig. 6 Residual stress distribution after three axial feeds. **a** Inner maximum principal stress

3 FEM model and formulation

Zhu et al. [22] optimized RFP by increasing the homogeneity of the product surface after forging and decreasing the damage and loading forge. Also, they used the Latin hypercube method. They employed a rigid plastic model for the simulation while this model does not have a high level of accuracy. Basically, there are three types of formulation for simulating metal formation through the finite element method: The first is the rigid plastic type; the second is the elastoplastic type; and the third is the viscoplastic type. Lee and Kobayashi developed the rigid plastic FEM. This approach is applied to simulating the upsetting of the cylinder, ring resizing, the extrusion process, and sheet bending. The rigid plastic model is generally used because it is simpler. For FEM, this simulation has been used as the explicit method because of the large deformations produced. Based on the boundary condition in FEM, the friction of process components is a fundamental item for providing an accurate model of the processes involved in forming metal. Thus, a spring-stiffness interrelation between the two contact areas has been assumed to handle the contact and friction of the tube and die, as well as the product and the mandrel. Moreover, in this simulation, it was assumed

Fig. 7 Plastic strain distribution after one axial feed. **a** Inner maximum principal strain. **b** Outer maximum principal strain

(a) Inner maximum principal strain.

(b) Outer maximum principal strain.

Table 6 Product geometry, contact force, and experimental results of radial forging

Sample type	Outer radius before process (mm)	Inner radius before process (mm)	Outer radius after process (mm)	Inner radius after process (mm)	Die force (KN)
Experiment	18	14.6	13.70	9.30	385.00
FEM	18	14.5	13.66	9.45	366.50

that (i) the material has viscoplastic behavior during the process; (ii) the forging process is isothermal in terms of heat transfer; and (iii) the dies and mandrel are assumed to be made from a rigid material. For the calculations and observations, RS has been defined as the final stresses on the product and as the residual stresses during the process. In most RFP simulations, the effects of die cooling are ignored due to the relatively short contact time between the die and the product.

The process geometry parameters are shown in Table 2. In RFP, the product is fed in after each stroke, which includes both rotary and axial feeds. The length of the product is 200 mm; and the parameters of motion and other processes are listed in Table 3.

For the simulation of processes in case of the flow rule, the von Mises yield criterion has been assumed. One form of the equilibrium equation has been used. The equation below is the final form of the basic equation for the simulation of the finite element:

$$[M^e]\{\ddot{\Delta}^e\} + [K^e]\{\Delta^e\} = \{F^e\} \tag{1}$$

where

$$[M^e] = \int_V \rho [N]^T [N] dV, [K^e] = \int_V [B]^T [C][B] dV \tag{2}$$

$$\{\Delta^e\} = \{u.v.w\}^T \tag{3}$$

Mass matrix $[M^e]$, stiffness matrix $[K^e]$, and mechanical loading $\{F^e\}$ have been calculated in Eq. (1). $[B]$ is the
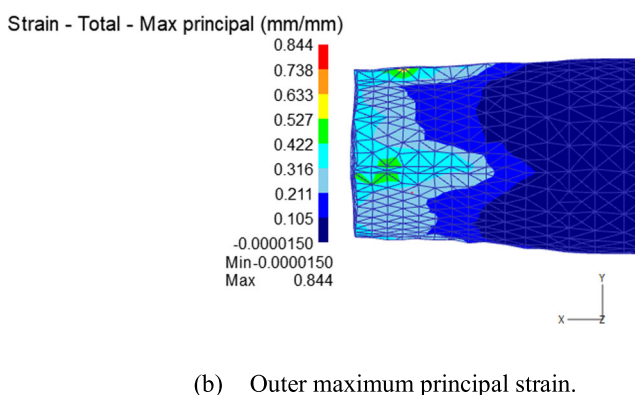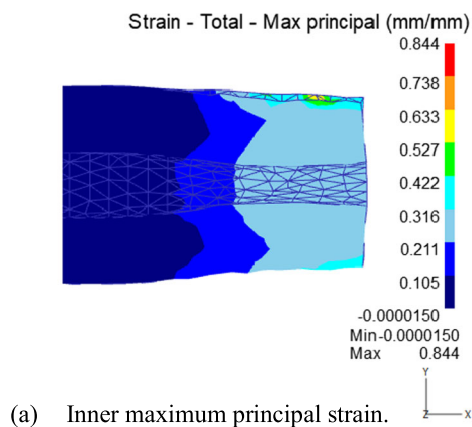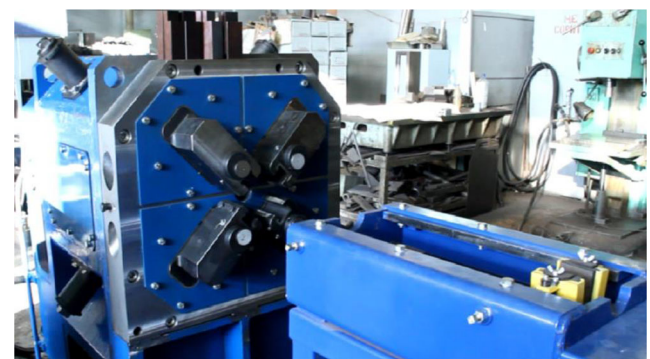

Fig. 8 Radial forging machine with a feeding system [23]

displacement matrix, $[C]$ is the elasticity matrix, N is the shape function, $\{u.\ v.\ w\}^T$ are the displacement components in a coordinate system, and ρ is the density. Heat transmission can be presented thusly:

$$[C_T^e]\{\dot{\theta}^e\} + [K_T^e]\{\theta^e\} = \{Q^e\} \qquad (4)$$

where

$$[C_T^e] = \int_V \rho c_p N^T N dV. \quad [K^e] = \int_V [B]^T [C][B]dV \qquad (5)$$

$$\{Q^e\} = \int_S N^T q dS + \int_V N^T r dV \qquad (6)$$

$[C_T^e]$ and $[K^e]$ show, respectively, the heat capacitation matrix and the conductive matrix. $\{Q^e\}$ is the external flux vector, c_p is the specific heat of the material, k is the thermal conductivity, and q and r are, respectively, the surface heat flux and the body heat flux caused by deformation. Hence, the couple thermal-stress equation can be written as

$$\begin{bmatrix} M & 0 \\ 0 & 0 \end{bmatrix}^e \left\{ \begin{matrix} \{\ddot{\Delta}\} \\ 0 \end{matrix} \right\}^e + \begin{bmatrix} 0 & 0 \\ 0 & C_T \end{bmatrix}^e \left\{ \begin{matrix} \{\dot{\Delta}\} \\ \{\dot{\theta}\} \end{matrix} \right\}^e$$

$$+ \begin{bmatrix} K_\Delta & K_{\Delta T} \\ K_{T\Delta} & K_T \end{bmatrix}^e \left\{ \begin{matrix} \{\Delta\} \\ \{\theta\} \end{matrix} \right\}^e$$

$$= \left\{ \begin{matrix} \{F\} \\ \{Q\} \end{matrix} \right\}^e$$

The friction model sticking state is $\tau = m\sigma_y / \sqrt{3}$, where m is the frictional coefficient and σ_y is the normal yield stress of the product material. Die, mandrel, and product contact are modelled through a penalty formulation. The sliding-sticking friction model has been utilized as a contact behavior. These frictions are shown in Table 4.

Frictional stress obeys Coulomb's law when this stress is less than the shear yield stress of the product material. For this reason, in the current study, the sliding-sticking friction or shear friction methods are assumed. As such, it is necessary to consider a 3D model, and the other simulation methods, such as an axisymmetric one, do not offer the same descriptive ability as the 3D model. Due to the very slight deformations of the mandrel and die in the process, it is assumed that these are made of rigid elements. Thus, the element number and mesh type of the FEM simulation of each section are shown in Table 5.

One of the aims of this investigation is to examine the behavior of the material in a viscoplastic condition at a high temperature and under a high level of strain. Due to these aims, it is assumed that nonlinear material will achieve the residual stress, plastic strain, and distribution of temperature in the axial and hoop directions during the last stage of the process. Also, the FEM simulation model derivation process has been illustrated in Fig. 4.
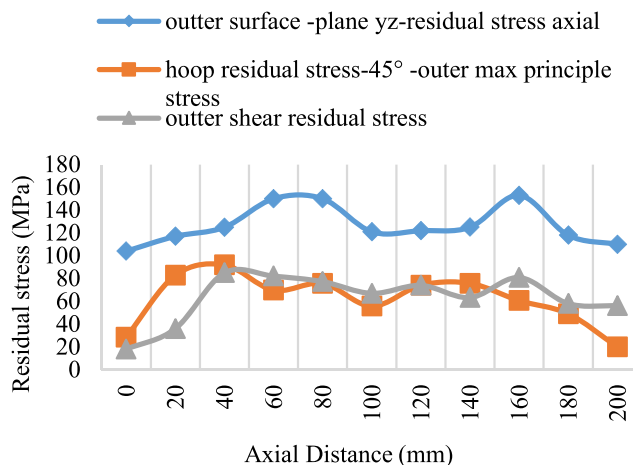

Fig. 9 Distribution of axial, hoop, and shear residual stresses on the outer surface along the tube length

In terms of die design, Ghaei and Movahhedy [11] imposed different die angles. In this study, a constant angle is used while the die angle is expected to affect the stress range. Two manipulators at both ends have been used within the process and the backpressure of spring is assumed for this gripper. The amount of material damage is a point in the integral value of the strain function, which affects the fracture tendency.

The cross-section of the strain effective area of the product during different strokes is expressed in Fig. 5. After the first pass of the second stroke, deformation is mainly created on the material forging area in contact with the dies.

Moreover, there is low non-homogeneous deformation on the material's outer surface due to the number of die strokes and the rotational rate feed of the tube. After the fifth stroke during the first pass, deformation on the outer surface decreases and the strain is transferred to the inner surface, around the mandrel. In the second pass of the second stroke, the smoothness of the surface improves, while the main strain is located on the outer surface but the amount of strain has decreased compared with step one. After the fifth stroke during
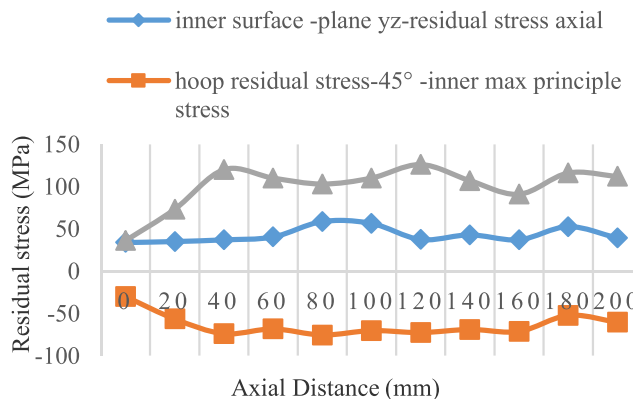

Fig. 10 Distribution of axial, hoop, and shear residual stresses on the inner surface along the tube length
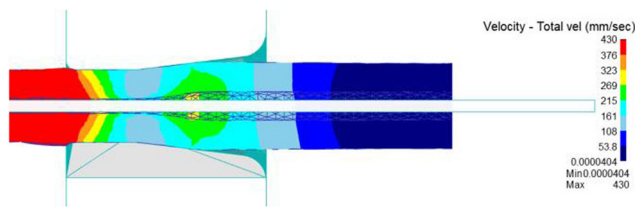
Fig. 11 Material flow velocity distribution at 100-mm distance (pass 1)

Fig. 13 Comparison of total force for different passes versus the axial direction

the second pass, there is a small gap around the mandrel, this will disappear at the end of the process.

4 Results and analysis

The results illustrate that the friction factor between the interfaces of RFP components has a considerable influence on the rate of residual stress. This stress is a significant criterion that can determine the longevity of a product. As such, RS contours and values have been achieved in this study.

Figure 6 shows the side section of the maximum principal stress on the inner and outer surfaces. The largest value of RS occurs on the outer layer. There is a non-uniform distribution of RS in the axial direction on the middle layer. Through comparison, the residual stresses on the three surface domains show that the outer surface may fail the material.

Due to this, die design can have a direct effect on product longevity.

It is obvious that as the stroke number increases, the plastic strain increases and the reduction in diameter will be significant. The maximum principal strain is shown in Fig. 7. The strain distribution is affected by the sinking and forging zones. Thus, the die angle can allow for the improvement of the principal strain and smoothness of the surface.

The geometric dimensions of the cold forging for experimental and FEM sample are presented in Table 6. As has been shown in the results, there is a good correspondence between the experimental and simulation results in the peak contact force through FEM simulations.

Thus, a comparison has been carried out based on the experimental results of RFP. The tests have been done by Metallurgical and Rotary Machines and Organizations of Machine-building Production in innovation enterprise Ural NITI (Ekaterinburg). The simulation results correspond with the empirical outcomes. The difference is less than 5%, which

might be due to a thermal effect. It can be concluded that the die loads dominate RS expansion and the effects of heat transfer were negligible in this process between die and tube (Fig. 8).

In Figs. 9 and 10, RS is displayed for the outer and inner surfaces of the tube, respectively. All stresses created along the product are almost uniform except in certain areas due to the clamp used to hold the product. The clamp prevents axial free deformation of the tube. Thus, in some areas, the stress in the segment increased in order to achieve a reduced tube radius. By comparing RS between the inner and outer layers, it is visible that the maximum stress range is created on the outer side in the axial direction [9].

The frictional force always acts in the opposite direction. It can also create RS in the axial and hoop directions. The spring-back effect of the tube in the radial direction might be one reason why tensile radial stress is created.

In Figs. 11 and 12, the distribution of the flow material velocity for passes 1 and 2, respectively, are shown. The velocity increases in pass 1 due to increasing strain. The friction coefficient and geometry parameters can influence the velocity. Increasing friction is expected to increase material velocity.

In regard to die pressure, the results of the forging load are presented according to die land length and axial feed per stroke. According to these results, it can be concluded that RS on the inner surface of the tube strongly depends on the
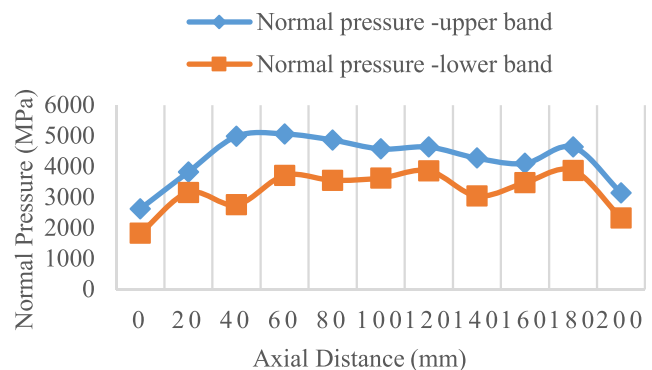

Fig. 12 Material flow velocity distribution at 100-mm distance (pass 2)

Fig. 14 Comparison of the upper and lower boundaries of the final (second) pass
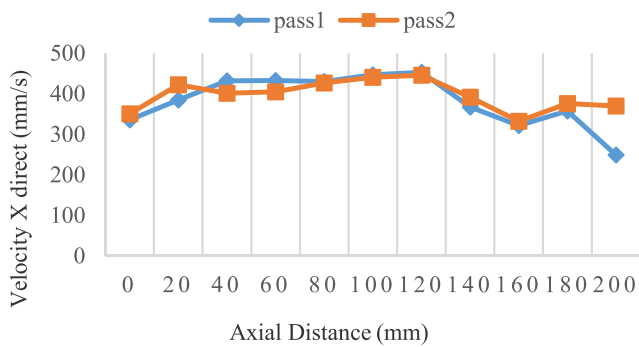
Fig. 15 Comparison of the product velocity in the axial direction for each pass

dimensions of the internal profiles of the mandrel and die. In Fig. 13, the total forces on the product over two passes have been illustrated. The results show that the total force during the first pass is higher than during the second one. This also confirms the expectations of the simulation.

In Fig. 14, the values of the upper and lower boundaries of the second pass are shown. The lower boundary expresses material damage in satisfying stress equilibrium. The minor difference between the two values is indicative of low damage to products and good yield criteria.

Figure 15 compares the velocity of the products in the axial direction. One of the main parameters for determining product
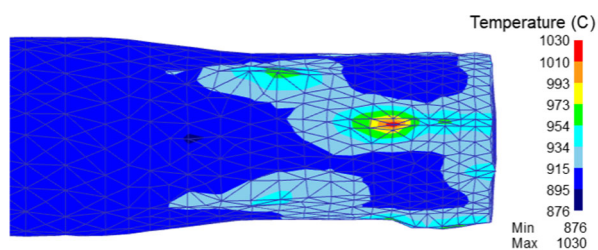
(a)   Outer temperature distribution.
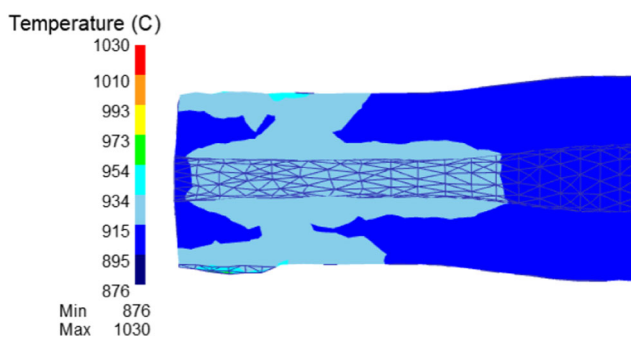
(b)   Inner temperature distribution.

Fig. 16 Temperature distribution for the inner and outer surfaces at 40 mm distance during the second pass. **a** Outer temperature distribution. **b** Inner temperature distribution

velocity is the friction coefficient. In this simulation, by assuming a constant coefficient, the result is in agreement with this supposition. Moreover, the velocity level can be used as a determinant parameter when designing manipulators.

Heat transfer between the environment, mandrel, die, and product has been considered to an appropriate degree of accuracy. The heat transfers such as conduction, convection, and radiation between process components are computed. In Fig. 16, the distribution temperature for the outer side during pass 1 is shown at a 40-mm distance.

5 Conclusion

In the current study, a 3D model base on FEM has been developed through simulation of RFP. The product was assumed to have viscoplastic behavior during the process. The simulation outcome showed the effect of axial spring stiffness on the forging load and material flow. The heat transfer and effect of friction on product velocity were also demonstrated. RS, the main parameter in this simulation, was illustrated during different passes. Using a comparison between experimental and simulation methods, the results obtained are validated. In fact, comparisons between experimental results and numerical analysis have been performed with the aim of verifying the accuracy of the matrixes used in the finite element method. Observing the good compatibility between these two results, it can be claimed that the matrixes used in the finite element method have good accuracy for simulation of RFP. Thus, these simulation results can be used in order to optimize the industrial operations condition. Based on this comparison, the results of this numerical model have been well-matched with the experimental results.

These results correspond well with the result of previous studies: they were fully based on the predictions of earlier investigations. The residual stresses indicate the validity and accuracy of the simulation. The results of this investigation can be summarized as follows:

- The peak RS of the material is located in the axial direction on the outer layers.
- Axial feed per stroke and die geometry are the most effective parameters for determining and validating the residual stresses.
- The maximum range of RS occurs in the first pass: the reduced diameter for each pass has been assumed to be constant.
- The distribution of RS on the outer and inner surfaces along the tube is uniform except at the two ends of the product.

References

1. Ameli A, Movahhedy MR (2007) A parametric study on residual stresses and forging load in cold radial forging process. Int J Adv

Manuf Technol 33:7–17. https://doi.org/10.1007/s00170-006-0453-2

2. Angelov T, Nedev A (1998) Numerical analysis of a hot-strip rolling problem with Coulomb-Siebel friction. Eng. Comput. (Swansea, Wales) 15:1000–1010. https://doi.org/10.1108/02644409810244101

3. Charni D, Ishkina S, Epp J, Herrrmann M, Schenck C, Zoch HW, Kuhfuss B (2018) Generation of residual stresses in rotary swaging process. MATEC Web Conf 190:1–9. https://doi.org/10.1051/matecconf/201819004001

4. Chen J, Chandrashekhara K, Mahimkar C, Lekakh SN, Richards VL (2012) Study of void closure in hot radial forging process using 3D nonlinear finite element analysis. Int J Adv Manuf Technol 62:1001–1011. https://doi.org/10.1007/s00170-011-3876-3

5. Chen J, Chandrashekhara K, Richards VL, Lekakh SN (2010) Three-dimensional nonlinear finite element analysis of hot radial forging process for large diameter tubes. Mater Manuf Process 25:669–678. https://doi.org/10.1080/10426910903536790

6. Choi SK, Chun MS, Van Tyne CJ, Moon YH (2006) Optimization of open die forging of round shapes using FEM analysis. J Mater Process Technol 172:88–95. https://doi.org/10.1016/j.jmatprotec.2005.09.010

7. Fajoui J, Kchaou M, Sellami A, Branchu S, Elleuch R, Jacquemin F (2018) Impact of residual stresses on mechanical behaviour of hot work steels. Eng Fail Anal 94:33–40. https://doi.org/10.1016/j.engfailanal.2018.07.020

8. Fan L, Wang Z, Wang H (2014) 3D finite element modeling and analysis of radial forging processes. J Manuf Process 16:329–334. https://doi.org/10.1016/j.jmapro.2014.01.005

9. T.I. G.Totten , M.Howes, Handbook of residual stress and deformation of steel - Google Kitaplar, 2002. https://books.google.com.tr/books?hl=tr&lr=&id=_a9UEHk4cOwC&oi=fnd&pg=PR6&dq=steel+quench+and+hardening+machine&ots=mi4equry4u&sig=VMF8UrKxm_pDXoNf9eaTetBGUmk&redir_esc=y#v=onepage&q=steelquenchandhardeningmachine&f=false

10. Ghaei A, Movahhedy MR, Taheri AK (2005) Study of the effects of die geometry on deformation in the radial forging process. J Mater Process Technol 170:156–163. https://doi.org/10.1016/j.jmatprotec.2005.04.100

11. Ghaei A, Movahhedy MR (2007) Die design for the radial forging process using 3D FEM. J Mater Process Technol 182:534–539. https://doi.org/10.1016/j.jmatprotec.2006.09.013

12. Huang J, Slater CD, Mandral A, Blackwell P (2017) A dynamic model for simulation of hot radial forging process. Procedia Eng 207:478–483. https://doi.org/10.1016/j.proeng.2017.10.808

13. Jang DY, Liou JH (1998) Study of stress development in axisymmetric products processed by radial forging using a 3-D non-linear finite-element method. J Mater Process Technol 74:74–82. https://doi.org/10.1016/S0924-0136(97)00252-5

14. Karunathilaka N, Tada N, Uemori T, Hanamitsu R, Kawano M (2018) Effect of contact pressure applied on tool surface during cold forging on fatigue life of tool steel. Procedia Manuf 15:488–495. https://doi.org/10.1016/j.promfg.2018.07.258

15. Khayatzadeh S, Poursina M, Golestanian H (2008) A simulation of hollow and solid products in multi-pass hot radial forging using 3D-FEM method. Int J Mater Form 1:371–374. https://doi.org/10.1007/s12289-008-0072-6

16. R. Koppensteiner, M. Auer, New forging drive system for radial forging based on double stroke mechanism Neues Antriebssystem für Radialschmiedemaschine basierend auf dem Doppelhubmechanismus, BHM Berg- Und Hüttenmännische Monatshefte 163 (2018) 361–366. doi: https://doi.org/10.1007/s00501-018-0760-6

17. Markov OE, Perig AV, Zlygoriev VN, Markova MA, Grin AG (2017) A new process for forging shafts with convex dies. Research into the stressed state. Int. J. Adv. Manuf. Technol 90:801–818. https://doi.org/10.1007/s00170-016-9378-6

18. Quagliato L, Kim D, Lee W, Berti GA, Lee C, Kim N (2017) Radial forging of aluminum to steel preform for the production of light-weighted wheel bearing outer race. Procedia Eng. 207:1683–1688. https://doi.org/10.1016/j.proeng.2017.10.922

19. Sanjari M, Karimi Taheri A, Ghaei A (2007) Prediction of neutral plane and effects of the process parameters in radial forging using an upper bound solution. J Mater Process Technol 186:147–153. https://doi.org/10.1016/j.jmatprotec.2006.12.029

20. Sanjari M, Saidi P, Karimi Taheri A, Hossein-Zadeh M (2012) Determination of strain field and heterogeneity in radial forging of tube using finite element method and microhardness test. Mater Des 38:147–153. https://doi.org/10.1016/j.matdes.2012.01.048

21. Wu Y, Dong X, Yu Q (2014) An upper bound solution of axial metal flow in cold radial forging process of rods. Int J Mech Sci 85:120–129. https://doi.org/10.1016/j.ijmecsci.2014.05.019

22. Zhu F, Wang Z, Lv M (2015) Multiobjective optimization of precision forging process parameters based on response surface method. Adv Mater Sci Eng 2015:1–7. https://doi.org/10.1155/2015/893730

23. Karamyshev AP, Nekrasov II, Parshin VS, Podolyak OO, Fedulov AA, Dronov AI et al (2014) The production of a machine designed for the cold radial cyclic forging of solid and tube billets. WIT Trans Ecol Environ 190:169–177. https://doi.org/10.2495/EQ140181